PNAS RESEARCH ARTICLE | EARTH, ATMOSPHERIC, AND PLANETARY SCIENCES

The effect of CO_2 ramping rate on the transient weakening of the Atlantic Meridional Overturning Circulation

Camille Hankel[a,b,1]

Edited by Eric Rignot, University of California, Irvine, CA; received June 9, 2024; accepted October 26, 2024

The Atlantic Meridional Overturning Circulation (AMOC) is a key component of the global climate that is projected to weaken under future anthropogenic climate change. While many studies have investigated the AMOC's response to different levels and types of forcing in climate models, relatively little attention has been paid to the AMOC's sensitivity to the rate of forcing change, despite it also being highly uncertain in future emissions scenarios. In this study, I isolate the AMOC's response to different rates of CO_2 increase in a state-of-the-art global climate model and find that the AMOC undergoes more severe weakening under faster rates of CO_2 change, even when the magnitude of CO_2 change is the same. I then propose an AMOC-ocean heat transport-sea ice feedback that enhances the decline of the circulation and explains the dependence on the rate of forcing change. The AMOC's rate-sensitive behavior leads to qualitatively different climates (including differing Arctic sea ice evolution) at the same CO_2 concentration, highlighting how the rate of forcing change is itself a key driver of global climatic change.

Atlantic Meridional Overturning Circulation | climate change | positive feedbacks

Significance

The Atlantic Meridional Overturning Circulation (AMOC) is an important ocean circulation that is expected to slow down under future anthropogenic climate change, with likely impacts on the climate of the North Atlantic region and beyond. In this study, I find that in a modern global climate model, the AMOC slows down more when the rate of atmospheric CO_2 change is faster, even when the level of CO_2 change is the same, and that this can be explained by a positive feedback cycle. This work highlights how the same amount of carbon emissions released over different amounts of time can lead to qualitatively different climates, making the timing of future emissions an important consideration for policy decisions.

The Atlantic Meridional Overturning Circulation (AMOC) is an important component of the large-scale ocean circulation that influences global climate through its transport of heat northward from the low to high latitudes, its ventilation of deep ocean waters, and its interactions with sea ice and atmospheric circulations. Early box models of the AMOC (e.g., refs. 1 and 2) exhibited multiple equilibria of the circulation, where the circulation could exist either in a strongly circulating or collapsed state for the same climate forcing (usually freshwater input into the North Atlantic). Since then, there have been concerns about the possibility of a future AMOC "tipping point," in which the AMOC abruptly collapses as it transitions from a strong steady state to a collapsed steady state after crossing a threshold under anthropogenic climate change. This has motivated a large body of literature aiming to examine the possibility of AMOC multiple equilibria and tipping points in ever-more sophisticated climate models (3–10) and to monitor ongoing changes in the Earth's AMOC (11–14), as rapid and irreversible changes in the circulation would have widespread implications on the regional and global climate. A weakened or collapsed AMOC is thought to impact not only local European temperatures and precipitation (e.g., refs. 15 and 16) but also the position of the midlatitude jet (17), ENSO variability and the position of the ITCZ (18, 19), and key modes of climate variability (20–23).

While a tipping point in the AMOC is related to a saddle-node bifurcation in its equilibrium behavior (a switch to a different equilibrium at some CO_2 level), more recent work has focused on how the circulation's out-of-equilibrium response to rapid climate change may also exhibit an abrupt weakening, even without a transition to a new steady state. In global climate models (GCMs) forced with an instantaneous or very rapid increase of either atmospheric CO_2 (e.g., refs. 9, 24, and 25) or freshwater input into the North Atlantic (so-called "hosing experiments," e.g., refs. 26–30), and run for a sufficiently long time to explore the circulation's equilibration to the forcing, different transient vs. equilibrium AMOC responses have been identified: The AMOC first undergoes a rapid decline toward a minimum on decadal to centennial timescales followed by a recovery to near-preindustrial strength on multicentennial to millennial timescales. Importantly, the full recovery of the circulation can occur even when the forcing is not reversed, as in ref. 24 where atmospheric CO_2 concentrations were abruptly quadrupled and held fixed for $\geq$1,000 y in several GCMs. This indicates that in such models, the AMOC's steady state at quadrupled CO_2 is hardly weaker than at preindustrial and that the initial rapid weakening of the circulation in such experiments represents a temporary deviation from this steady state. The physical mechanisms of the AMOC's recovery have been investigated previously. Some studies invoke the build-up

Author affiliations: [a]Cooperative Institute for Climate, Ocean, and Ecosystem Studies, University of Washington, Seattle, WA 98105; and [b]Department of Atmospheric and Climate Science, University of Washington, Seattle, WA 98195

Author contributions: C.H. designed research; performed research; analyzed data; and wrote the paper.

The author declares no competing interest.

This article is a PNAS Direct Submission.

[1]Email: crhankel@uw.edu.

This article contains supporting information online at https://www.pnas.org/lookup/suppl/doi:10.1073/pnas.2411357121/-/DCSupplemental.

Published December 23, 2024.

of a large positive salinity anomaly in the South Atlantic during the period of weakened AMOC which reinvigorates the circulation once it gets advected northward (29, 31, 32). Others cite the eventual subtropical subsurface warming that occurs on multicentennial timescales and reestablishes the large-scale meridional density gradient (24, 28). Such recovery mechanisms can also be thought of as slow, negative feedbacks that make the AMOC stable and relatively insensitive to perturbations of intermediate magnitude.

The presence of slow, stabilizing feedbacks implies that the AMOC may be sensitive to the rate of forcing change that drives it: if the rate of forcing change is faster than the timescale of AMOC-stabilizing mechanisms, then the AMOC may respond more severely than if the forcing were changed more gradually on the same timescales as the stabilizing mechanisms. While the response of the AMOC to different magnitudes of forcing has been studied extensively, the potential sensitivity of the AMOC to different rates of forcing change has received much less attention, especially in studies that use state-of-the-art fully coupled climate models. In a conceptual box model of the AMOC, Alkhayuon et al. (33) identified a so-called "rate-induced tipping point," where the circulation undergoes a transition to a collapsed state at a critical rate of freshwater forcing change, even though the forcing magnitude had not passed the bifurcation threshold for the tipping point. Stocker and Schmittner (34) used a zonally averaged three-basin ocean model to show that the AMOC collapsed permanently in more rapid CO_2 ramping experiments and weakened transiently under more gradual CO_2 changes. Only two CO_2 ramping rates were used for a given magnitude of CO_2 change, and it is unclear if the model was integrated long enough for the observed AMOC collapse to be considered "permanent" (i.e., a new AMOC steady state reached). Finally, using a primitive but three-dimensional coupled ocean-atmosphere model, Stouffer and Manabe (35) explored the response of the global climate system, including the AMOC, to five different rates of CO_2 increase to twice preindustrial levels ($2\times CO_2$). They found that slower ramping rates achieved greater weakening of the AMOC by the time of CO_2 doubling, but only two simulations were run longer with fixed CO_2, leaving the circulation's full (transient and equilibrium) dependence on the CO_2 ramping rate unclear. The timescales of integration needed to probe both the transient and equilibrium response of the AMOC to forcing likely depend on the exact model used, but for fully coupled GCMs, it appears that at least multiple millennia are needed (24). At a minimum, the AMOC strength evolution should reach a quasi-equilibrium state by the end of integration, though some previous work suggests that the deep ocean continues to evolve long after such a cutoff, for up to 10,000 y (e.g., ref. 36). Thus, both the insufficient simulation time and idealized nature of previous modeling studies on the AMOC's response to rates of forcing limit the applicability of their conclusions to the Earth's climate system. Furthermore, previous studies have yet to provide a mechanistic explanation for any "rate-sensitivity" of the AMOC that may exist.

Given that the rate at which we will approach net-zero carbon emissions—not only the level of final greenhouse concentrations—is highly uncertain, I have identified a need to isolate and understand the AMOC's dependence on the CO_2 ramping rate in modern, state-of-the-art GCMs. To do so, I use the Community Earth System Model version 1.2.2 (CESM) and perform several experiments in which the atmospheric CO_2 concentration is ramped to the same final CO_2 magnitude over different lengths of time, and then is held fixed for over a thousand years until the AMOC appears to reach a quasi-equilibrium. I find that the level of transient AMOC weakening depends on the rate of CO_2 ramping, with more rapid ramping rates leading to more severe weakening on the multicentennial timescale—a result not captured by the shorter model simulations performed in earlier work (34, 35). I then analyze North Atlantic ocean density changes across the ramping experiments to identify an AMOC-ocean heat transport-sea ice feedback that enhances the AMOC weakening and whose strength is sensitive to the rate of CO_2 change. This work demonstrates in a modern GCM that the same amount of CO_2 emitted over different amounts of time can have substantially different impacts on the weakening of the AMOC and the various climate phenomena that it interacts with (such as Arctic sea ice), a conclusion that has substantial implications for how we evaluate the cost of future carbon emissions scenarios.

Results

Fig. 1 shows the AMOC's response to doubling the atmospheric CO_2 concentration at seven different ramping rates in the global climate model (CESM1; see *Materials and Methods*). It reveals that in all experiments, the AMOC experiences a transient weakening before a subsequent recovery to its preindustrial strength, consistent with other literature performing long model simulations (e.g., refs. 8, 24, 27, 29, 30, and 32). These experiments also reveal that for ramping rates of 0.5% CO_2 increase per year and slower, the level of transient weakening depends on the ramping rate, with faster ramping rates causing more severe weakening, including some weakening that occurs after CO_2 concentrations stop increasing. At ramping rates $\geq$0.5%/year, the level of transient weakening is similar across different rates, suggesting that the rate-dependent effect saturates as the response approaches that of an instantaneous CO_2 doubling experiment (shown in the black dashed line). Current actual rates of CO_2 increase are estimated to be slightly higher than 0.5%/year. The nature of the circulation's recovery is also different across the experiments, with the more rapid ramping experiments also undergoing a more abrupt recovery than the gradual ramping

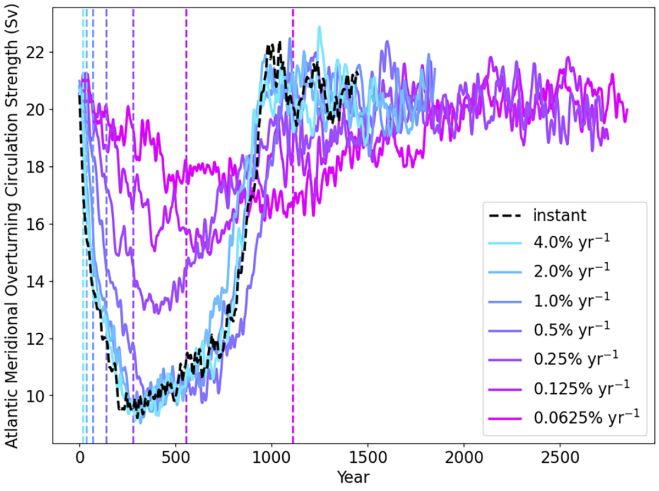

Fig. 1. Strength of the AMOC (maximum streamfunction value between the equator and 65 °N and below 250 m in depth) in eight different experiments that increase CO_2 up to two times preindustrial levels at the ramping rates given in the legend, with 10-y linear smoothing applied twice to filter out year-to-year variability. Vertical dashed lines indicate the year when twice preindustrial CO_2 concentrations ($2\times CO_2$) were reached for each experiment, after which CO_2 is held fixed.

experiments. This may be consistent with previous proposals of a low-latitude build-up of a salinity anomaly and an eventual northward advection of this anomaly as the AMOC recovery mechanism (e.g., ref. 29): the more severe decline of the AMOC in rapid ramping experiments would allow for a larger build-up of salinity, and therefore a more rapid recovery once this anomaly is advected to the North Atlantic. The rest of this work focuses on understanding why the level of transient weakening depends on the ramping rate, which has not been previously identified or explained.

To explain the dependence of the AMOC's weakening on the rate of CO_2 change, I propose a positive AMOC-ocean heat transport-Arctic sea ice feedback that enhances the AMOC weakening when the CO_2 ramping rate is faster. This feedback is illustrated in Fig. 2. To start off this feedback, enhanced warming over the North Atlantic, driven by increased CO_2, leads to a reduced large-scale meridional ocean density gradient and an initial weakening of the AMOC (Step 1 in Fig. 2). As the AMOC typically carries substantial heat to the high latitudes, this initial weakening leads to a reduction in northward ocean heat transport (OHT) across 60 °N (Step 2), causing a cooling of sea surface temperatures in the sub-Arctic/North Atlantic and Arctic sea ice regrowth (despite elevated CO_2 levels, Step 3). This subsequently leads to increased export of ice out of the Arctic and into the North Atlantic, where the exported ice melts and provides a major source of surface freshwater forcing on the ocean (Step 4). This freshwater reduces the North Atlantic ocean density further (Step 5), and in turn, weakens the AMOC further. Importantly, under more gradual CO_2 ramping, the upper ocean has more time to come into equilibrium with the greenhouse forcing and is transiently warmer at a given CO_2 level than the rapid ramping experiment. Consequently, some of the ocean heat transport decline due to the circulation's decline is compensated for by an increase in the heat content of the transported waters. Thus, in the more gradual ramping experiments, there is less decline in the ocean heat transport (Step 2G), less high-latitude cooling, no sea ice regrowth (Step 3G), and no additional freshwater input into the North Atlantic from sea ice. This leads to a more modest feedback, and less overall AMOC weakening under more gradual CO_2 ramping rates than under rapid rates. The subsequent Results sections provide evidence for each step of this feedback cycle.

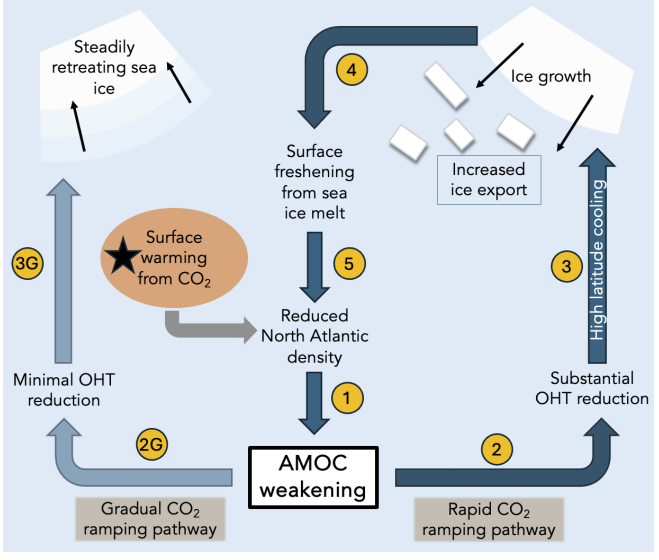

Fig. 2. Schematic showing the proposed positive feedback cycle that can enhance AMOC weakening. The initial perturbation to the system by CO_2 forcing is indicated by the black star. Steps 1 to 5 indicate the path taken by the rapid CO_2 ramping experiment, resulting in enhanced AMOC weakening via the AMOC-OHT-sea ice feedback described above. Steps 1, 2G, and 3G indicate the alternate path taken by the gradual CO_2 ramping experiment that does not result in extra AMOC weakening.

Ocean Density Contributions to AMOC Weakening. I analyze the causes of AMOC weakening by examining changes in ocean densities across the experiments. Recently, several studies have shown that the basin-wide overturning streamfunction can be accurately reconstructed from large-scale meridional ocean density gradients, using various forms of a so-called "rotated" thermal wind relation (24, 29, 36–39). While the correspondence of the reconstructed streamfunction with the actual streamfunction does not necessarily mean that the associated ocean density gradients are the cause of the AMOC changes (as they may instead be responding to AMOC changes), such an approach helps identify important differences in the ocean's evolution across the ramping experiments in this work. Here, I use the method of Butler et al. (38) to transform the large-scale Atlantic meridional density gradient into a basin-wide overturning streamfunction value as a function of depth by performing a double vertical integral (*Materials and Methods*). The large-scale meridional density gradient is defined as the difference between the average ocean density in a basin-wide North Atlantic box spanning 40 °N–65 °N and a South Atlantic box spanning 34 °S–40 °N, similar to ref. 36. The region of isopycnal outcropping and deep convection—a key area for driving AMOC changes—is therefore captured in the North Atlantic box, which helps produce an accurate and interpretable reconstruction of the circulation (24, 36). The reconstructed AMOC strength captures between 71% and 89% of the raw magnitude of AMOC weakening across the experiments (without smoothing) and shows very good temporal correspondence to the actual AMOC strength index on decadal–multicentennial timescales (*SI Appendix*, Fig. S1).

The success of the streamfunction reconstruction from average ocean density changes in the North Atlantic and South Atlantic boxes suggests that one may look at these regions to understand the key differences across ramping experiments. For simplicity, I examine only the period of AMOC decline in the two endmember ramping experiments (the first 964 y of the 0.0625% CO_2 change per year experiment and the first 290 y of the 4%/year experiment), and look at the bulk density gradient changes (vertically averaged between 500 m and 2,500 m depth) which also scale remarkably well with the AMOC strength. From this, I find that South Atlantic densities actually strengthen the (positive) meridional gradient due to ocean warming that reduces the densities there, and do by around 27% more in the rapid experiment than in the gradual experiment (*SI Appendix*, Fig. S2), suggesting that the South Atlantic cannot explain the extra weakening of the AMOC in the rapid experiment. On the other hand, the North Atlantic bulk density changes weaken the meridional density gradient by ≈50% more in the rapid experiment compared to the gradual (*SI Appendix*, Fig. S2), outweighing the contributions of the South Atlantic and indicating that the North Atlantic dominates the mechanisms of the rate-sensitive AMOC slowdown. This is consistent with the majority of previous literature that finds reductions in North Atlantic density to be a mechanism of future AMOC slowdowns and even uses freshwater input to the North Atlantic in models to induce and study an AMOC collapse (e.g., refs. 26, 30, and 40).

Next, I attribute the North Atlantic density reductions (which weaken the meridional density gradient) to temperature and salinity changes (*Materials and Methods*). Fig. 3 shows the contributions of temperature and salinity to ocean density changes (from preindustrial) in the North Atlantic for the most gradual and rapid ramping experiments as a function of ocean depth and time. In Fig. 3*A*, we see that ocean temperatures steadily warm in the gradual ramping experiment and reduce the North Atlantic ocean density throughout the period of AMOC decline. Gradual freshening also occurs in Fig. 3*C*, though it contributes less to the overall reduction of density. On the other hand, Fig. 3*D* shows that the rapid ramping experiment starts to develop a very strong surface freshwater anomaly around year 50 that penetrates to depths of 2,000 m and persists until around year 200, at which point the surface signal continues to increase but no longer penetrates to the subsurface. We can deduce that the subsurface freshening is likely due to increased surface freshwater input (rather than increased subsurface freshwater transport) for two reasons: first, because the subsurface freshwater anomalies visibly seem to be continuous in space and time with the surface anomalies, and second, because the total ocean freshwater transport across 40 °N into the North Atlantic box is actually decreasing during this time (*SI Appendix*, Fig. S10). That these density changes appear to be forced by surface freshwater changes suggests that they are a driver of, rather than a response to, AMOC changes. The causes of surface freshening in both experiments will be diagnosed in the following section. Meanwhile, Fig. 3*B* shows an overall much stronger subsurface warming in the rapid experiment (especially between 300 m and 2,000 m and starting around year 200) that contributes substantially to the stronger reduction in density in the rapid vs. the gradual experiment. Importantly, this strong warming signal does not extend all the way to the surface, and in fact, sits entirely below a surface cooling signal and below the strong freshening signal seen in Fig. 3*D* during this same time period. I hypothesize, consistent with previous literature (39, 41, 42), that the surface freshening seen in Fig. 3*D* creates a light, freshwater surface layer whose positive buoyancy causes it to sit stably above the warmer (but saltier) subsurface layer. This freshwater "cap" as it is called, prevents the subsurface waters from mixing with the surface and cooling to the cold, North Atlantic atmosphere as they would normally without such a stable surface layer. Further evidence for this is that the total northward ocean heat transport into the North Atlantic decreases substantially during this time, suggesting that the warm subsurface signal cannot be due to an increase in ocean heat transport. *SI Appendix*, Fig. S3 confirms the overall relative contributions of temperature and salinity to density changes by examining their bulk (vertically averaged) values: by the end of the period of AMOC decline, additional ocean warming is entirely responsible for the rapid experiment's more substantial North Atlantic density decline compared to the gradual experiment, but during an intermediate period (approximately years 75 to 175) increased freshening in the rapid experiment is equally, if not more important than warming. Thus, while the gradual experiment's AMOC decline corresponds with steady decreasing North Atlantic densities due mainly to gradual warming, the additional AMOC weakening in the rapid experiment corresponds with additional surface freshening which both directly reduces the bulk ocean density and indirectly reduces it by suppressing heat loss to the atmosphere. These results provide evidence for Step 1 of the proposed feedback (AMOC weakening due to North Atlantic warming) and Step 5 (additional AMOC weakening due to North Atlantic surface freshening) but invoke the question: where does the additional freshening signal come from and why does it appear only in the rapid ramping experiment?

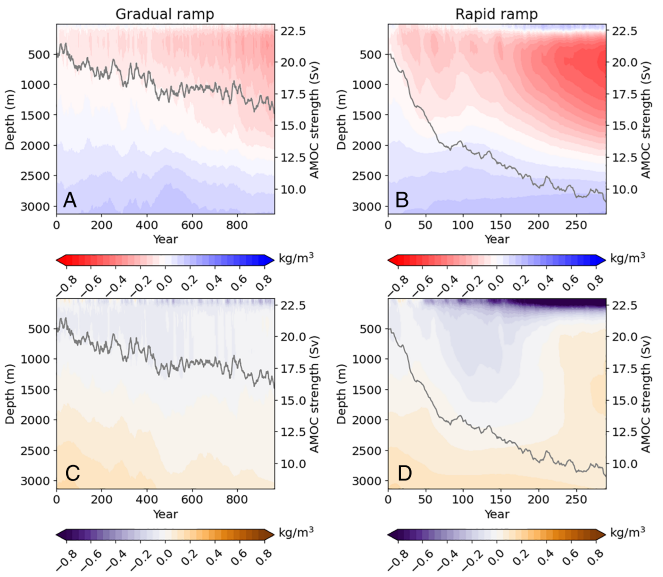

Fig. 3. Changes in the North Atlantic average density compared to preindustrial due to temperature (panels *A* and *B*) and salinity (panels *C* and *D*) in the two endmember ramping experiments (left column: 0.0625% CO_2 increase per year, right column: 4% per year). The gray line indicates the AMOC strength using the right y-axis.

Causes of North Atlantic Surface Freshening. To answer this question, I perform a decomposition of the net surface freshwater forcing over the North Atlantic box used in the AMOC reconstruction. Fig. 4 shows the net surface freshwater flux in the black lines and the three nonnegligible components that contribute to it over the periods of AMOC weakening for gradual and rapid ramping experiments. The gradual ramping experiment has a relatively modest, negative change in total surface freshwater forcing (Fig. 4*A*, black line), while the rapid experiment displays a positive change in total surface freshwater forcing over the period shown (Fig. 4*B*). This qualitatively different evolution of surface freshwater fluxes is driven by differing meltwater input from sea ice in the two experiments, shown in the blue lines in Fig. 4 *A* and *B*. While the gradual experiment shows a gradual decline of sea ice meltwater flux into the ocean, the sea ice meltwater flux evolution in the rapid experiment is more complex, first decreasing sharply, before increasing steadily from years 50 to 250 and driving the total surface freshwater flux up. This provides evidence that Step 5 in the feedback cycle in Fig. 2 is indeed driven by increasing sea ice melt in the North Atlantic. Examining the sea ice evolution itself (Fig. 4 *C* and *D*) reveals that it closely parallels the evolution of the sea ice meltwater flux. While total Arctic sea ice volume steadily declines in the gradual experiment, the rapid ramping experiment exhibits an initial period of ice loss, followed by an unexpected period of sea ice regrowth that lasts for nearly 200 y. The total Arctic sea ice volume eventually starts to decrease again in the rapid ramping experiment, achieving the same equilibrium sea ice state as the gradual experiment by the end of the simulation (see *SI Appendix*, Fig. S4 for all experiments' full timeseries of Arctic sea ice volume). The period of sea ice regrowth is reflected in the local (North Atlantic) ice evolution of the rapid experiment

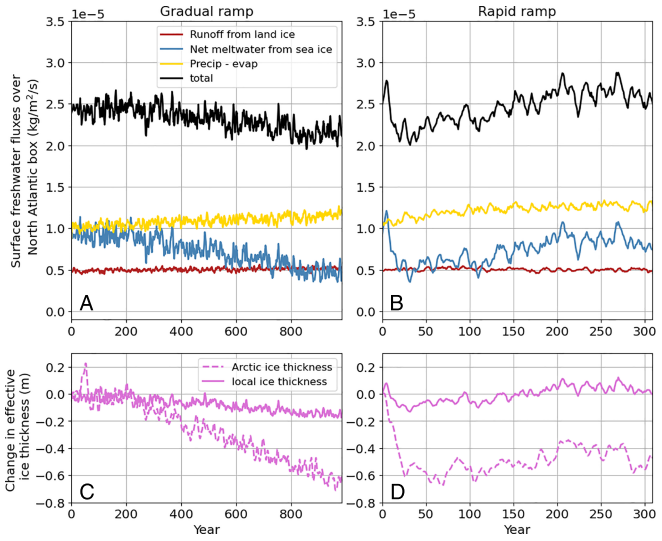

Fig. 4. Surface freshwater forcing budget over the North Atlantic box for the most gradual (*A*) and most rapid (*B*) ramping experiments. Not pictured are contributions from two processes that have near-zero values: frazil ice formation and brine rejection. Local (average over the North Atlantic box above 50 °N) and Arctic-wide (average above 50 °N) "effective" sea ice thickness (ice volume divided by region area) over the same period for the most gradual (panel *C*) and rapid (panel *D*) experiments.

as well, which closely matches the evolution of the local sea ice meltwater flux.

While the positive relationship between local sea ice volume and the sea ice meltwater flux may seem surprising, it can be explained by the balance of dynamic and thermodynamic contributions to sea ice volume. During the period of sea ice regrowth in the rapid experiment, there is an enhancement of thermodynamic ice growth in the high Arctic (in the Arctic Ocean basin), i.e., freeze-up of new ice due to colder conditions (which will be explained later). This is accompanied by an enhancement of dynamic ice loss (mechanical export of ice out of Baffin Bay/Denmark Strait) from this region. The North Atlantic is on the receiving end of this ice transport, experiencing an increase in dynamic ice import, and an accompanying increase in thermodynamic loss (local melting) of ice that supplies the increased surface freshwater flux seen in Fig. 4*B* and which in turn weakens the meridional density gradient. This process is depicted in *SI Appendix*, Fig. S5, which shows a map of the change in dynamic and thermodynamic contributions to ice volume loss/growth over this period of ice regrowth in the rapid experiment, confirming that there is an increase in ice melting in various regions of the North Atlantic that are close to the sea ice edge. This analysis supports Step 4 of the proposed feedback cycle, in which Arctic sea ice growth leads to an increase in surface freshening from sea ice melt through the mechanism of enhanced sea ice export to the North Atlantic.

Causes of Arctic Sea Ice Regrowth. Next, I diagnose the causes of the regional cooling that lead to enhanced sea ice growth and freshwater input into the North Atlantic in the rapid experiment but not the gradual. By looking at the spatial pattern of cooling that develops in the rapid experiment, I note that the cooling initially occurs off the southeast coast of Greenland, precisely over the region of deep ocean convection that marks the terminus of the AMOC, before spreading further into the Arctic (*SI Appendix*, Figs. S6 and S7). This suggests that the cooling may be tied to the decline in AMOC strength itself because the AMOC typically transports significant heat from the low latitudes into the North Atlantic region. Indeed, the total northward ocean heat transport (OHT) across 60 °N decreases by nearly 0.2 PW during the period of AMOC decline in the rapid ramping experiment, but by only about 0.05 PW in the gradual experiment (*SI Appendix*, Fig. S9), providing a likely cause for the cooling and sea ice regrowth in the rapid experiment. A similar mechanism has been invoked by Lee and Liu (43) to argue that present-day sea ice loss may have been more severe in the absence of ongoing AMOC weakening. This process explains Steps 3 and 4 in Fig. 2, closing the loop of the positive feedback on AMOC strength in the rapid experiment: surface warming of the North Atlantic under increased CO_2 causes an initial decline in AMOC strength, which in turn leads to a reduction of ocean heat transport into the Arctic, high latitude cooling, large-scale ice growth, an increase in sea ice export to the North Atlantic, and finally an increase in sea-ice meltwater input into the ocean that further weakens the AMOC.

The main other possible cause of high-latitude cooling would be changes in the surface atmospheric heat fluxes over the region. The total (clear-sky plus cloud) longwave downwelling does decrease substantially during the period of Arctic cooling in the rapid ramping experiment (by $\approx$7 W/m^2 on average in the area above 60 °N, with changes mostly coming from the clear-sky component). However, the changes in LW downwelling radiation are quite spatially narrow and appear to be highly correlated with the pattern of sea surface temperature cooling, suggesting that they are likely a response to, rather than a driver of, surface cooling (*SI Appendix*, Fig. S8). Net shortwave radiation received by the surface also declines (by about 2 W/m^2 on average in the region above 60 °N) during this period, suggesting that initial sea-ice regrowth could kick off an ice-albedo feedback that enhances the basin-wide cooling and ice growth.

Sensitivity of Ocean Heat Transport to the Rate of CO_2 Increase. Finally, I analyze why this positive AMOC-OHT-sea ice feedback mechanism acts so much more effectively in the rapid ramping experiment compared to the gradual experiment. To do so, it is helpful to consider the time periods over which the two experiments exhibit similar AMOC declines due to similar causes (North Atlantic temperature changes) and identify any key differences that allow these two experiments to subsequently diverge. Fig. 5*A* shows the total northward OHT across 60 °N versus the AMOC strength over such periods (*Materials and Methods*) for the two end-member ramping experiments and a least squares regression for each dataset. This reveals that the OHT in the more gradual ramping experiment is less sensitive to AMOC weakening than in the rapid ramping experiment. In other words, not only does the OHT decline by less in the gradual ramping experiment overall (which could be explained by differing levels of total AMOC weakening), but it also declines by less for the same amount of AMOC weakening when compared to the rapid ramping experiment. By bootstrapping the linear regression, I obtain distributions for the estimates of the two regression slopes and find them to be both different than 0 at a statistically significant level and importantly different from each other at a significant level as well (their distributions have zero overlap with 10,000 iterations, Fig. 5*B*). Therefore, we can infer that the positive feedback on AMOC weakening may occur less strongly in the gradual ramping experiment because it experiences a smaller decline in northward OHT than the rapid experiment for a similar level of initial AMOC weakening, explaining the divergence of Steps 2 and 2G in Fig. 2. The minimal reduction of OHT in the gradual

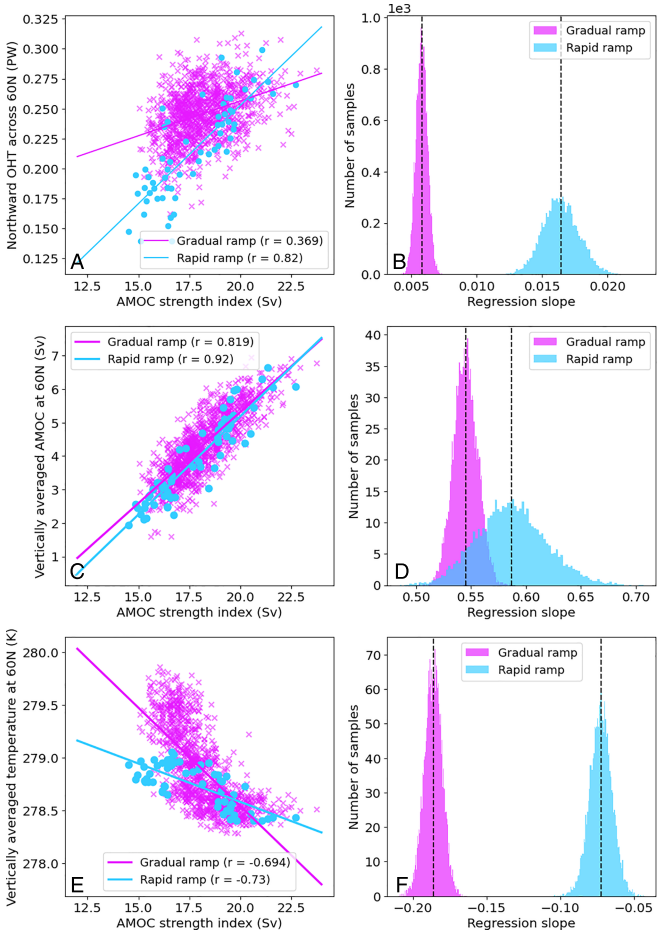

Fig. 5. Northward ocean heat transport and its components (ocean temperature and streamfunction) over similar periods of AMOC decline for the two endmember experiments. Panel (*A*) shows the northward ocean heat transport across 60 °N versus the AMOC strength index for the gradual experiment in magenta (first 1,097 y of the simulation) and the rapid experiment in blue (first 61 y) and a least squares regression fit to each experiment. Panel (*B*) shows the distribution of the bootstrapped least squares regression slope for both experiments using the same colors. Panels (*C*) and (*D*) are the same as a and b, but for the spatially averaged overturning streamfunction in a cross section at 60 °N vs. the AMOC strength index. Panels (*E*) and (*F*) are the same but for the spatially averaged ocean temperature in a cross section at 60 °N. Black dashed vertical lines in panels *B*, *D*, and *F* indicate the mean regression slope for the given data.

experiment prevents widespread North Atlantic/Arctic cooling, sea ice regrowth, and additional surface freshwater anomalies from developing.

The evolution of northward OHT across 60 °N could be different in the two experiments for two reasons: differing evolutions of meridional volumetric transport and differing evolutions of ocean temperature/heat content. Ideally, one would decompose the changes in northward OHT into these two contributions; however, because the net meridional flow across 60 °N is not zero (due to net flow across the Bering Straight), this decomposition can lead to spurious results. Instead, I regress the two variables that contribute to OHT—the average overturning streamfunction and ocean temperature at 60 °N—onto the AMOC strength to estimate which of the two variables evolve differently in the two ramping experiments for the same amount of AMOC decline. These regressions are not meant to imply a causal relationship between either variable and the AMOC, but rather to show on average, how much the ocean temperature and the overturning streamfunction change at 60 °N over comparable periods of AMOC decline in the two experiments. The results of this analysis are shown in Fig. 5 *C*–*F*. Panel (*C*) shows the vertically averaged meridional overturning streamfunction at 60 °N regressed onto the AMOC strength index for both experiments. While the rapid experiment does experience more decline in the streamfunction at 60 °N for the same decline in the AMOC index, the estimated uncertainties on the regression slopes are substantially overlapping (Fig. 5*D*), making their difference not statistically significant ($P = 0.10$). This means that we cannot conclude that the streamfunction at 60 °N changes more in the rapid experiment for the same amount of AMOC strength decline, and therefore cannot assert that it contributes to differences in OHT between the two experiments. On the other hand, Fig. 5*E* shows that the rapid ramping experiment undergoes less average ocean warming at 60 °N than the gradual experiment and that this difference is statistically significant (the uncertainty on the estimates of the two regression slopes is entirely nonoverlapping, Fig. 5*F*). In other words, there is a smaller increase in ocean heat content at 60 °N in the rapid experiment for the same amount of AMOC decline.

The different evolutions of ocean temperature over similar periods of AMOC decline are a manifestation of an important general feature of the experiments: the more gradual experiments have more time to equilibrate to the CO_2 forcing, with, for example, the 0.0625%/year experiment exhibiting around 1 K more global mean surface temperature warming than the 4%/year experiment at the time of CO_2 doubling. The result is that in the gradual ramping experiment, some of the OHT reduction that would have occurred due to reduced volumetric transport is compensated for by an increase in the heat content of the transported waters. This is also true for the more rapid ramping experiment but to a statistically significant lesser degree. This reveals that a simple, intuitive difference between the ramping experiments—that the slower components of the climate system including subsurface ocean temperatures are much more in equilibrium with CO_2 forcing—can likely explain some of the AMOC's sensitivity to rates of CO_2 change by modulating the response of ocean heat transport to AMOC weakening. With a more modest reduction in OHT under more gradual ramping, there is less cooling in the North Atlantic, no sea ice regrowth or extra surface meltwater input, and the positive feedback on AMOC weakening is suppressed. That the evolution of the streamfunction at 60 °N is estimated to be different in the two ramping experiments (though not to a statistically significant degree) suggests that the spatial structure of the circulation's decline could still play a secondary role in modulating the ocean heat transport evolution and therefore the strength of the proposed feedback under different CO_2 ramping rates. This analysis of OHT changes provides an explanation for why the proposed feedback on AMOC weakening is sensitive to the rate of forcing.

Discussion

In this study, I have identified that the AMOC's level of weakening depends on the rate of change of CO_2 in a fully coupled global climate model. This rate dependence of the AMOC's response to forcing occurs when the magnitude of CO_2 change is equal across experiments. In seeking to explain this rate-sensitivity, I proposed a positive feedback that enhances AMOC weakening under more rapid rates of CO_2 ramping. In this feedback, an initial AMOC weakening driven by warming North

Atlantic waters causes a decline in northward ocean heat transport (OHT), which in turn causes high latitude cooling, Arctic sea ice regrowth, and an increase in ice export out of the Arctic. The additional exported ice then melts in the North Atlantic near the terminus of the AMOC, which further weakens the circulation by introducing a negative surface (freshwater) density anomaly. Crucially, in more gradual CO_2 ramping scenarios, the reduction in northward OHT is much more modest because the upper ocean temperature has more time to come into equilibrium with the CO_2 forcing, partially offsetting the decline in volumetric transport by increasing the upper ocean heat content. This makes the overall feedback cycle weaker and the magnitude of the AMOC decline smaller in the more gradual ramp.

This study was in part motivated by recent work highlighting the possibility of rate-induced tipping points in the Earth system (33, 44–46), where a premature transition to a different steady state occurs at a critical rate of forcing change even when no bifurcation threshold has been crossed. No such critical rates were found in this study, perhaps because the magnitude of forcing change itself was not large enough to cause a complete AMOC collapse (as indicated by the instantaneous CO_2 doubling experiment), or because the model is not one that supports multiple AMOC equilibrium states (discussed more below). Whether or not the mechanism found here would operate similarly at higher CO_2 values depends on several factors. For example, the crucial regrowth of sea ice after $2\times CO_2$ is reached in rapid ramping experiments may not occur if the Arctic is substantially warmer and far away from the freezing point at the end of ramping. On the other hand, more substantial increases in net precipitation minus evaporation over the Atlantic may occur in higher CO_2 ramping experiments, adding a new time-dependent forcing on the ocean density whose net effect on the feedback mechanism found here is unknown. Future work could explore whether the mechanism discussed here leads to rate-induced tipping points in the AMOC at higher CO_2 levels using the same experimental setup designed here or using ocean-only models forced with a wide variety of surface forcing scenarios.

The identification of multicentennial periods of Arctic sea ice regrowth and an associated temporary erasure of Arctic amplification that can occur after halting greenhouse gas emissions is an important finding of this study that has not to my knowledge been explored previously. Such periods of Arctic sea ice regrowth would likely have significant impacts on nearby human and ecological systems and thus merit further study. This work also identified a relationship between Arctic sea ice and the AMOC—where sea ice growth actually weakens the AMOC further—that to some extent contradicts previous studies that find Arctic sea ice loss to weaken the AMOC (e.g., refs. 47–49). This highlights how the exact forcing scenarios used to study future AMOC slowdowns (e.g., freshwater forcing, CO_2 changes, regional radiative forcing, or albedo perturbations) impact theAMOC-sea ice relationship and the mechanisms of a circulation slowdown.

There are a few caveats that should be considered when interpreting what the rate-sensitivity of the AMOC in CESM1 means for the Earth's AMOC. The model's representation of the AMOC dynamics may differ from the Earth's AMOC due to the parameterization of mesoscale and submeso-scale eddy velocities and associated heat transports. While the model's eddy component of the overturning streamfunction is very small, any modifications to the ocean heat transport that would occur from directly resolving smaller spatial scales could affect the strength or existence of the proposed feedback. It has also been proposed that biases in the net freshwater transport into the Atlantic exhibited by many GCMs could lead to an overly stable AMOC in such models by modifying the sign of the salt-advective feedback (27, 50–53). In this configuration of CESM1, the net freshwater transport by the overturning circulation is biased slightly positive relative to observations (*SI Appendix*, Fig. S11), but still yields the correct sign of the salt-advective feedback. The negative value of the net freshwater transport supports the use of CESM1 to study the AMOC's stability and time-dependent response to forcing, and according to the literature, suggests that the AMOC could collapse permanently in this model for larger forcing magnitudes (10, 54–58).

The coarse resolution configuration of CESM1 used here is also known to be cold-biased in its representation of the preindustrial mean-state climate by around 0.75 K for the globally averaged surface temperature. Several aspects of the climate mean state are thought to impact the AMOC's sensitivity to forcing, including the mean state of the AMOC itself (59, 60), the mean state of the western subpolar gyre (61), and the mean state of Arctic sea ice (62). In particular, the amount and timing of Arctic sea ice loss and regrowth—a key aspect of the positive feedback mechanism—could be different when starting from a warmer mean-state climate. Therefore, some of the quantitative aspects of the results presented here should not be interpreted as projections for the Earth's AMOC under future CO_2 increases (e.g., the exact level of AMOC weakening under a given ramping rate, the rate of CO_2 increase at which the AMOC's response becomes insensitive).

The relevance of the AMOC-OHT-sea ice feedback proposed here to the Earth's climate system would be further supported by evidence that the feedback exists across different global climate models, particularly those run with higher horizontal resolution. In *SI Appendix*, Figs. S12 and S13, I compare some results from this work to abrupt CO_2 doubling experiments conducted for two other models (CNRM-CM6-1 and CESM2) as part of the Coupled Model Intercomparison Project 6 (CMIP6). While the full feedback cycle cannot be analyzed due to insufficient integration time (only 150 y) and incomplete variable output, both CMIP6 models exhibit North Atlantic density reductions caused by surface freshening and subsurface warming, similar to CESM1 (*SI Appendix*, Fig. S12). They also both exhibit a period of sea ice regrowth in the North Atlantic, potentially enhancing the sea ice meltwater into the ocean, as in CESM1 (*SI Appendix*, Fig. S13). These results indicate that the proposed AMOC-OHT-sea ice feedback may enhance AMOC weakening across different models, though its importance relative to other mechanisms in these models would require additional simulations.

Finally, the findings of this work have significant implications for how we evaluate future emissions scenarios to inform policy decisions. While commonly used policy metrics such as the Social Cost of Carbon take into account the rate of CO_2 increase insofar as it impacts the global mean surface temperature, they do not account for the fact that the same level of warming could imply qualitatively different climates. This study reveals the possibility of appreciably different Arctic sea ice volume and North Atlantic sea surface temperatures (with a probable impact on Northern European temperatures) under the same level of CO_2 increase. Downstream, this means that the "social cost" of emitting the same amount of carbon over different periods could be vastly different in ways that have not been anticipated. Beyond the scope of the AMOC's sensitivity to CO_2 ramping rates, this work reveals the imperative of studying the entire climate system's response to different rates of forcing if we are to accurately

understand and evaluate the consequences of a range of future forcing scenarios.

Materials and Methods

Model. The ramping experiments are conducted with a fully coupled configuration of CESM version 1.2.2. The atmospheric model is CAM4, which has 26 vertical levels that are defined on a hybrid sigma–pressure grid. The ocean model (POP2) has 60 vertical levels defined in depth. I use a relatively coarse resolution horizontal grid–3.5 degrees in the atmosphere and 3.7 degrees in the ocean (T35g37)–due to the computational limitations of running such long and numerous experiments. The model is spun up for 2500 years with fixed preindustrial conditions ($CO_2 = 284.7$ ppm), at which point even the deep ocean is fairly close to a quasi-equilibrium. In light of the concerns about the influence of model resolution on the AMOC (63, 64), *SI Appendix*, Fig. S14 shows that the magnitude of the AMOC's decline and the North Atlantic sea surface cooling signal under 1%/year CO_2 increases appear to be similar across 1-degree and 3.5-degree model resolutions.

Experimental Design. From the spun-up model state, eight experiments are conducted in which the concentration of atmospheric CO_2 is increased to twice preindustrial levels (569.4 ppm) over different periods of time and then is held fixed at 569.4 ppm until the AMOC appears to reach a steady state. The length of the eight experiments therefore varies depending on the time to reach one doubling of CO_2 and the time it takes the AMOC to recover. One of these experiments consists of an instantaneous doubling, while the other seven consist of an exponential ramping of CO_2 concentration at rates ranging from 0.0625% increase per year to 4% increase per year. This equates to a linear ramping of the CO_2 radiative forcing that occurs over periods between 18 and 1,109 y.

AMOC Index. The index used to indicate the strength of the AMOC is defined here as the maximum of the zonally averaged total streamfunction in the Atlantic (the sum of Eulerian mean, eddy-induced, and submesoscale components of the "MOC" variable in CESM output) between the equator and 65 °N and below a depth of 250 m. I evaluate this maximum at the monthly timescale so that the AMOC index tracks the maximum streamfunction throughout the year, and then I generate a yearly averaged timeseries. Excluding values above 250 m serves to exclude the subtropical gyres from the calculation. The index is insensitive to the exact latitude range considered so long as it spans the true streamfunction maximum location (typically around 35 °N).

AMOC reconstruction. Following Butler et al. (38), the AMOC strength index can be reconstructed from the large-scale meridional density gradient in the Atlantic. The basic premise of the reconstruction is a so-called rotated thermal wind relationship. Under thermal wind balance, meridional velocity shear (in the vertical) is linearly related to zonal density gradients, but by assuming that meridional density gradients scale linearly with zonal gradients, one can write the rotated thermal wind expression as

$$\frac{\partial V}{\partial z} = \frac{cg}{f_0 \rho_0 L_y} \rho_y(z),$$

where V is the basin-wide velocity, ρ_0 and f_0 are mean values of density and the Coriolis parameter, L_y is the length scale of the basin, $\rho_y = \rho(NA) - \rho(SA)$ is the basin-wide meridional density gradient described below, and c is a dimensionless parameter representing the scaling between the zonal and meridional density gradients. This expression can be integrated vertically to yield:

$$V(z) = \frac{cg}{\rho_0 f_0 L_y} \left(\frac{1}{h} \int_{-h}^{0} \left(\int_{z'}^{0} \rho_y(z'')dz'' \right) dz' - \int_{z}^{0} \rho_y(z')dz' \right),$$

where h is the ocean's depth and the constant of integration is determined by requiring net-zero meridional flow across the basin. Finally, an expression for the meridional overturning streamfunction as a function of depth can be obtained by performing another vertical integral, yielding:

$$\Psi(z) = L_x \int_{z}^{0} V(z')dz',$$

where Ψ represents the streamfunction. The scaling factor c is tuned to optimize the match under preindustrial conditions (average over the last 20 y of the spin-up run) between the reconstructed streamfunction and the "true" basin-wide overturning streamfunction, taken as the maximum streamfunction value at each level over a latitude range of 0 to 65 °N.

While Butler et al. (38) use small North and South Atlantic boxes confined to within 10° longitude of the western ocean boundary, I opt to use much larger regions to calculate large-scale meridional density gradient, approximately following refs. 36 and 24. The North Atlantic box spans 40 °N to 65 °N and the full width of the Atlantic, while the South Atlantic box spans 34 °S to 40 °N. The meridional density gradient is calculated as the difference between the vertical profiles of the horizontally averaged density in these two boxes. Using the western boundary boxes of Butler et al. (38) to estimate the large-scale meridional density gradient does not qualitatively change the results, but the success of this approach could be sensitive to the exact location of the western boundary current in a given model. To estimate the contributions of temperature and salinity separately to North Atlantic density changes, I use the Gibbs Seawater Oceanographic Toolbox python package (65, which utilizes the nonlinear equation of state) to calculate the hypothetical ocean density if only temperature had changed (using the preindustrial salinity profiles) and if only salinity had changed (using the preindustrial temperature profiles).

Analysis of Ocean Heat Transport. The "period of similar AMOC decline" for the two endmember ramping experiments is defined: 1) for the gradual ramping as all the years leading up to the AMOC strength minimum (first 1,097 y of the simulation), and 2) for the rapid ramping experiment as the years leading up to when its smoothed AMOC timeseries (10-y linear smoothing twice applied) reaches the same level of AMOC weakening as the gradual experiment's AMOC minimum (this corresponds to the first 61 y of the rapid simulation). The average ocean temperature at 60 °N over these time periods is calculated as a two-dimensional spatial average (in longitude and depth) over a zonal cross section of the Atlantic ocean at 60 °N. The average overturning streamfunction at 60 °N is calculated as an average over depth only, since the model output variable (MOC) is already zonally averaged.

Data, Materials, and Software Availability. Model data and python code used to generate the results and figures in this work can be found at Zenodo (66).

ACKNOWLEDGMENTS. I thank Carl Wunsch and Eli Tziperman for their helpful feedback, and Jon Proctor and Kaitlyn Loftus for their aesthetic input. This work was supported by NSF Grant 2303486 of the Paleo Perspective on Present and Projected Climate program, National Center for Atmospheric Research Small Exploratory Computing Grant UHAR0020, and the Cooperative Institute for Climate, Ocean, and Ecosystem Studies Postdoctoral Fellowship Program.

1. H. Stommel, Thermohaline convection with two stable regimes of flow. *Tellus* **13**, 224–230 (1961).
2. R. X. Huang, J. R. Luyten, H. M. Stommel, Multiple equilibrium states in combined thermal and saline circulation. *J. Phys. Oceanogr.* **22**, 231–246 (1992).
3. S. Manabe, R. J. Stouffer, Two stable equilibria of a coupled ocean-atmosphere model. *J. Clim.* **1**, 841–866 (1988).
4. S. Rahmstorf, Bifurcations of the Atlantic thermohaline circulation in response to changes in the hydrological cycle. *Nature* **378**, 145–149 (1995).
5. A. Schiller, U. Mikolajewicz, R. Voss, The stability of the north Atlantic thermohaline circulation in a coupled ocean-atmosphere general circulation model. *Clim. Dyn.* **13**, 325–347 (1997).
6. E. Hawkins *et al.*, Bistability of the Atlantic overturning circulation in a global climate model and links to ocean freshwater transport. *Geophys. Res. Lett.* **38**, L10605 (2011).
7. P. Wu, J. Ridley, A. Pardaens, R. Levine, J. Lowe, The reversibility of co_2 induced climate change. *Clim. Dyn.* **45**, 745–754 (2015).
8. L. Jackson, R. Wood, Hysteresis and resilience of the AMOC in an eddy-permitting GCM. *Geophys. Res. Lett.* **45**, 8547–8556 (2018).

9. D. Rind *et al*., Multicentury instability of the Atlantic meridional circulation in rapid warming simulations with GISS ModelE2. *J. Geophys. Res.: Atmos.* **123**, 6331–6355 (2018).
10. R. M. van Westen, M. Kliphuis, H. A. Dijkstra, Physics-based early warning signal shows that AMOC is on tipping course. *Sci. Adv.* **10**, eadk1189 (2024).
11. B. I. Moat *et al*., Atlantic meridional overturning circulation observed by the RAPID-MOCHA-WBTS (RAPID-Meridional Overturning Circulation and Heatflux Array-Western Boundary Time Series) array at 26N from 2004 to 2022 (v2022.1) (NERC EDS British Oceanographic Data Centre NOC, 2023). https://doi.org/10.5285/223b34a3-2dc5-c945-e063-7086abc0f274. Accessed 12 March 2024.
12. E. Frajka-Williams *et al*., Atlantic meridional overturning circulation: Observed transport and variability. *Front. Mar. Sci.* **6**, 260 (2019).
13. E. L. Worthington *et al*., A 30-year reconstruction of the Atlantic meridional overturning circulation shows no decline. *Ocean Sci.* **17**, 285–299 (2021).
14. Y. Fu *et al*., Seasonality of the meridional overturning circulation in the subpolar North Atlantic. *Commun. Earth Environ.* **4**, 181 (2023).
15. L. Jackson *et al*., Global and European climate impacts of a slowdown of the AMOC in a high resolution GCM. *Clim. Dyn.* **45**, 3299–3316 (2015).
16. K. Bellomo *et al*., Impacts of a weakened AMOC on precipitation over the Euro-Atlantic region in the EC-Earth3 climate model. *Clim. Dyn.* **61**, 3397–3416 (2023).
17. W. Liu, A. V. Fedorov, S. P. Xie, S. Hu, Climate impacts of a weakened Atlantic meridional overturning circulation in a warming climate. *Sci. Adv.* **6**, eaaz4876 (2020).
18. A. Timmermann *et al*., The influence of a weakening of the Atlantic meridional overturning circulation on ENSO. *J. Clim.* **20**, 4899–4919 (2007).
19. B. Orihuela-Pinto, A. Santoso, M. H. England, A. S. Taschetto, Reduced ENSO variability due to a collapsed Atlantic meridional overturning circulation. *J. Clim.* **35**, 5307–5320 (2022).
20. R. Zhang, T. L. Delworth, Impact of the Atlantic multidecadal oscillation on north pacific climate variability. *Geophys. Res. Lett.* **34**, L23708 (2007).
21. R. Zhang *et al*., A review of the role of the Atlantic meridional overturning circulation in Atlantic multidecadal variability and associated climate impacts. *Rev. Geophys.* **57**, 316–375 (2019).
22. M. E. Hamouda, C. Pasquero, E. Tziperman, Decoupling of the Arctic Oscillation and North Atlantic Oscillation in a warmer climate. *Nat. Clim. Change* **11**, 137–142 (2021).
23. C. Deser, On the teleconnectivity of the "Arctic Oscillation". *Geophys. Res. Lett.* **27**, 779–782 (2000).
24. D. B. Bonan, A. F. Thompson, E. R. Newsom, S. Sun, M. Rugenstein, Transient and equilibrium responses of the Atlantic overturning circulation to warming in coupled climate models: The role of temperature and salinity. *J. Clim.* **35**, 5173–5193 (2022).
25. P. Nobre *et al*., AMOC decline and recovery in a warmer climate. *Sci. Rep.* **13**, 15928 (2023).
26. C. Bitz, J. Chiang, W. Cheng, J. Barsugli, Rates of thermohaline recovery from freshwater pulses in modern, last glacial maximum, and greenhouse warming climates. *Geophys. Res. Lett.* **34**, L07708 (2007).
27. L. Jackson, Shutdown and recovery of the AMOC in a coupled global climate model: The role of the advective feedback. *Geophys. Res. Lett.* **40**, 1182–1188 (2013).
28. M. D. Thomas, A. V. Fedorov, Mechanisms and impacts of a partial AMOC recovery under enhanced freshwater forcing. *Geophys. Res. Lett.* **46**, 3308–3316 (2019).
29. R. K. Haskins, K. I. Oliver, L. C. Jackson, S. S. Drijfhout, R. A. Wood, Explaining asymmetry between weakening and recovery of the AMOC in a coupled climate model. *Clim. Dyn.* **53**, 67–79 (2019).
30. L. C. Jackson *et al*., Understanding AMOC stability: The North Atlantic hosing model intercomparison project. *Geosci. Model Dev. Discuss.* **2022**, 1–32 (2022).
31. P. Wu, L. Jackson, A. Pardaens, N. Schaller, Extended warming of the northern high latitudes due to an overshoot of the Atlantic meridional overturning circulation. *Geophys. Res. Lett.* **38**, L24704 (2011).
32. L. Ackermann, C. Danek, P. Gierz, G. Lohmann, AMOC recovery in a multicentennial scenario using a coupled atmosphere-ocean-ice sheet model. *Geophys. Res. Lett.* **47**, e2019GL086810 (2020).
33. H. Alkhayuon, P. Ashwin, L. C. Jackson, C. Quinn, R. A. Wood, Basin bifurcations, oscillatory instability and rate-induced thresholds for Atlantic meridional overturning circulation in a global oceanic box model. *Proc. R. Soc. A* **475**, 20190051 (2019).
34. T. F. Stocker, A. Schmittner, Influence of CO_2 emission rates on the stability of the thermohaline circulation. *Nature* **388**, 862–865 (1997).
35. R. J. Stouffer, S. Manabe, Response of a coupled ocean-atmosphere model to increasing atmospheric carbon dioxide: Sensitivity to the rate of increase. *J. Clim.* **12**, 2224–2237 (1999).
36. M. F. Jansen, L. P. Nadeau, T. M. Merlis, Transient versus equilibrium response of the ocean's overturning circulation to warming. *J. Clim.* **31**, 5147–5163 (2018).
37. M. Nikurashin, G. Vallis, A theory of the interhemispheric meridional overturning circulation and associated stratification. *J. Phys. Oceanogr.* **42**, 1652–1667 (2012).
38. E. Butler, K. Oliver, J. J. M. Hirschi, J. Mecking, Reconstructing global overturning from meridional density gradients. *Clim. Dyn.* **46**, 2593–2610 (2016).
39. R. K. Haskins, K. I. Oliver, L. C. Jackson, R. A. Wood, S. S. Drijfhout, Temperature domination of AMOC weakening due to freshwater hosing in two GCMs. *Clim. Dyn.* **54**, 273–286 (2020).
40. R. J. Stouffer *et al*., Investigating the causes of the response of the thermohaline circulation to past and future climate changes. *J. Clim.* **19**, 1365–1387 (2006).
41. J. Gregory *et al*., A model intercomparison of changes in the Atlantic thermohaline circulation in response to increasing atmospheric CO_2 concentration. *Geophys. Res. Lett.* **32**, L12703 (2005).
42. P. Bakker *et al*., Fate of the Atlantic Meridional Overturning Circulation: Strong decline under continued warming and Greenland melting. *Geophys. Res. Lett.* **43**, 12–252 (2016).
43. Y. C. Lee, W. Liu, The weakened Atlantic meridional overturning circulation diminishes recent arctic sea ice loss. *Geophys. Res. Lett.* **50**, e2023GL105929 (2023).
44. C. W. Arnscheidt, D. H. Rothman, Routes to global glaciation. *Proc. R. Soc. A* **476**, 20200303 (2020).
45. U. Feudel, Rate-induced tipping in ecosystems and climate: The role of unstable states, basin boundaries and transient dynamics. *Nonlinear Process. Geophys.* **30**, 481–502 (2023).
46. P. D. L. Ritchie, H. Alkhayuon, P. M. Cox, S. Wieczorek, Rate-induced tipping in natural and human systems. *Earth Syst. Dyn.* **14**, 669–683 (2023).
47. F. Sévellec, A. V. Fedorov, W. Liu, Arctic sea-ice decline weakens the Atlantic Meridional Overturning Circulation. *Nat. Clim. Change* **7**, 604–610 (2017).
48. H. Li, A. Fedorov, W. Liu, AMOC stability and diverging response to Arctic sea ice decline in two climate models. *J. Clim.* **34**, 5443–5460 (2021).
49. B. S. Ferster, A. Simon, A. Fedorov, J. Mignot, E. Guilyardi, Slowdown and recovery of the Atlantic Meridional Overturning Circulation and a persistent north Atlantic warming hole induced by Arctic Sea ice decline. *Geophys. Res. Lett.* **49**, e2022GL097967 (2022).
50. W. Liu, S. P. Xie, Z. Liu, J. Zhu, Overlooked possibility of a collapsed Atlantic Meridional Overturning Circulation in warming climate. *Sci. Adv.* **3**, e1601666 (2017).
51. J. Mecking, S. Drijfhout, L. Jackson, M. Andrews, The effect of model bias on Atlantic freshwater transport and implications for AMOC bi-stability. *Tellus A* **69**, 1299910 (2017).
52. R. M. van Westen, H. A. Dijkstra, Asymmetry of AMOC hysteresis in a state-of-the-art global climate model. *Geophys. Res. Lett.* **50**, e2023GL106088 (2023).
53. R. M. Van Westen, H. A. Dijkstra, Persistent climate model biases in the Atlantic ocean's freshwater transport. *Ocean Sci.* **20**, 549–567 (2024).
54. S. Rahmstorf, On the freshwater forcing and transport of the Atlantic thermohaline circulation. *Clim. Dyn.* **12**, 799–811 (1996).
55. P. de Vries, S. L. Weber, The Atlantic freshwater budget as a diagnostic for the existence of a stable shut down of the meridional overturning circulation. *Geophys. Res. Lett.* **32** (2005).
56. H. A. Dijkstra, Characterization of the multiple equilibria regime in a global ocean model. *Tellus A* **59**, 695–705 (2007).
57. S. E. Huisman, M. Den Toom, H. A. Dijkstra, S. Drijfhout, An indicator of the multiple equilibria regime of the Atlantic Meridional Overturning Circulation. *J. Phys. Oceanogr.* **40**, 551–567 (2010).
58. W. Weijer *et al*., Stability of the Atlantic Meridional Overturning Circulation: A review and synthesis. *J. Geophys. Res.: Oceans* **124**, 5336–5375 (2019).
59. A. J. Weaver, M. Eby, M. Kienast, O. A. Saenko, Response of the Atlantic Meridional Overturning Circulation to increasing atmospheric CO_2: Sensitivity to mean climate state. *Geophys. Res. Lett.* **34**, L05708 (2007).
60. Y. J. Lin, B. E. Rose, Y. T. Hwang, Mean state AMOC affects AMOC weakening through subsurface warming in the Labrador Sea. *J. Clim.* **36**, 3895–3915 (2023).
61. L. C. Jackson *et al*., Impact of ocean resolution and mean state on the rate of AMOC weakening. *Clim. Dyn.* **55**, 1711–1732 (2020).
62. A. Levermann, J. Mignot, S. Nawrath, S. Rahmstorf, The role of northern sea ice cover for the weakening of the thermohaline circulation under global warming. *J. Clim.* **20**, 4160–4171 (2007).
63. M. J. Roberts *et al*., Sensitivity of the Atlantic Meridional Overturning Circulation to model resolution in CMIP6 HighResMIP simulations and implications for future changes. *J. Adv. Model. Earth Syst.* **12**, e2019MS002014 (2020).
64. P. Chang *et al*., An unprecedented set of high-resolution earth system simulations for understanding multiscale interactions in climate variability and change. *J. Adv. Model. Earth Syst.* **12**, e2020MS002298 (2020).
65. T. J. McDougall, P. M. Barker, Getting started with TEOS-10 and the Gibbs seawater (GSW) oceanographic toolbox. *SCOR/IAPSO WG* **127**, 1–28 (2011).
66. C. Hankel, Data and code for "The effect of CO_2 ramping rate on the transient weakening of the Atlantic Meridional Overturning Circulation". Zenodo. https://doi.org/10.5281/zenodo.14219963. Deposited 26 November 2024.